ACCEPTED VERSION

Ching-Tai Ng, Siu-Kui Au
Mode shape scaling and implications in modal identification with known input

Final publication at http://dx.doi.org/10.1016/j.engstruct.2017.11.017

---

http://hdl.handle.net/2440/124271

Mode shape scaling and implications in modal identification with known input

Ching-Tai Ng[1] and Siu-Kui Au[2]

[1] School of Civil, Environmental & Mining Engineering, The University of Adelaide, SA 5005, Australia

[2] Center for Engineering Dynamics and Institute for Risk and Uncertainty, University of Liverpool, L69 3GH, Liverpool, United Kingdom

Abstract

This study proposes a mode shape scaling and parameterization scheme for modal identification with known input. Through the derivation of the equations for known input modal identification using the proposed mode shape scaling and parameterization scheme, the study provides insight into the relationship between the identified modal parameters and information required in the forced vibration test. In typical applications of modal identifications, when there is sufficient amount of data, the formulation using the proposed mode shape scaling and parameterization scheme shows that it allows modal parameters to be determined efficiently in a globally identifiable manner. An illustrative example using synthetic data is provided in this study. The findings show that an appropriate mode shape scaling and normalization scheme could reduce the information required in the modal identification procedure for some modal parameters, i.e. natural frequencies, damping ratios and mode shapes. This significantly simplifies the procedure of the forced vibration test, and hence, it can be carried out in a more robust manner.

1. Introduction

Modal identification is a technique that allows extraction of the modal parameters, such as natural frequencies, damping ratios, and mode shapes, of a structure from measured vibration data [1]. The identified modal parameters can then be used for structural model updating [2] and damage detection [3]. In the last decade, vibration tests have been carried out different on different types of structures, e.g. bridge [4], tower [5] and building [6].

Forced vibration test makes use of a special device, such as shaker or impact hammer, to produce vibration response of structures for identifying modal properties. Memari et al. [7] carried out a forced vibration study on a six story steel frame building during the construction stage. The forced vibration was carried out when steel frames, floor slabs and some of the walls were completed. An unbalanced mass exciter was installed at the roof of the building to induce the excitation. Natural frequencies, damping ratios and mode shapes were identified from the measured acceleration data. Halling et al [8] conducted a forced vibration test on a concrete deck steel girder bridge. An eccentric mass shaking machine was used to generate the required excitation on the bridge. The study identified the natural frequencies and mode shapes. These identified modal parameters were also used to update a finite element model of the bridge. Burgueno et al. [9] carried out a forced vibration test on a fiber reinforced polymer (FRP) composite bridge. They employed a long stroke electro-dynamic force generator to excite the bridge and the measured acceleration data was used to identify the natural frequencies and mode shapes.

Although more demanding in terms of budget and logistics, it has several advantages over free [10] or ambient vibration tests. Essentially, the signal-to-noise ratio of data can be significantly improved and the information of input excitation can significantly reduce the identification uncertainty of modal parameters [11]. In typical applications, the location and direction of the artificial excitation is assumed to be known, although in some cases it is difficult to control them in field testing conditions [12].

The objective of this study is to demonstrate that an appropriate mode shape scaling scheme can reduce the information required in the modal identification procedure for some modal parameters, such as natural frequencies, damping ratios and mode shapes, allowing forced vibration tests to be performed in a more robust manner. A mode shape scaling and parameterization scheme is first proposed, which allows modal parameters to be determined efficiently in a globally identifiable manner. Based on this scheme, implications on the required information in the modal identification are discussed. A Bayesian context is assumed as it allows uncertainties to be fundamentally quantified, but the implications on identifiability are general and applicable to other non-Bayesian or deterministic approaches.

Section 2 first summarizes the formulation of the known input modal identification. Section 3 proposes the mode shape scaling and parameterization scheme and its formulation of the known input modal identification. Section 4 discusses the relationship between modal identification and the information of the exciter configuration. Section 5 presents the formulation of the Bayesian approach under the proposed mode shape scaling and parameterization scheme. Insights and practical aspects are discussed in Section 6. Section 7 presents an illustrative example. Finally, conclusions are provided in Section 8.

2. Modal identification with known single input

Consider a multi-degree-of-freedom (MDOF) structure satisfying the dynamic equation:

$$\mathbf{M}\ddot{\mathbf{x}}(t) + \mathbf{C}\dot{\mathbf{x}}(t) + \mathbf{K}\mathbf{x}(t) = \mathbf{F}(t) \tag{1}$$

where $\mathbf{M}$, $\mathbf{C}$ and $\mathbf{K}$ are respectively the conventional mass, damping, stiffness matrices; and $\mathbf{F}(t)$ is the force vector. With mass normalization, the i-th modal force is given by

$$p_i(t) = \frac{\boldsymbol{\varphi}(i)^T \mathbf{F}(t)}{\boldsymbol{\varphi}(i)^T \mathbf{M}\boldsymbol{\varphi}(i)} \tag{2}$$

and $\boldsymbol{\varphi}(i) \in R^n$ is the (partial) mode shape vector of the i th mode confined to the n measured dofs. Without loss of generality, suppose the acceleration response of the structure is measured at n

degrees of freedom (dofs). Assuming m contributing modes, the measured data in the frequency domain can be modeled as

$$\mathcal{F}_k = \sum_{i=1}^{m} \boldsymbol{\varphi}(i) h_{ik} P_{ik} + \boldsymbol{\varepsilon}_k \tag{3}$$

where $\mathcal{F}_k$ is the fast Fourier transform (FFT) of measured data at frequency $\mathrm{f}_k = k/N\Delta t$ (Hz); N is the number of samples per data channel; Δt is the time step; P_{ik} is the FFT of the modal force at k-th frequency; $\boldsymbol{\varepsilon}_k$ is the prediction error (e.g., measurement noise). For a given mode i, h_{ik} is the transfer function between modal excitation and modal acceleration:

$$h_{ik} = -\left[\left(\beta_{ik}^2 - 1\right) + \mathbf{i}\left(2\zeta_i\beta_{ik}\right)\right]^{-1} \tag{4}$$

where $\beta_{ik} = f_i/\mathrm{f}_k$ is a frequency ratio; $\mathbf{i}^2 = -1$. f_i (Hz) and ζ_i are respectively the natural frequency and damping ratio.

During testing measurement, suppose the structure is subjected to a single dominant source of artificial excitation that is also measured. Depending on the direction of the applied excitation on the structure, the force can be distributed to more than one dof. For convenience in analysis, assume without loss of generality that the force on the j th measured dof is given by $ma_j s(t)$, where m (kg) is a nominal mass value (e.g., moving mass of a shaker), a_j is a dimensionless factor accounting for the contribution of force to the dof, which has value between $0-1$, and it is zero on other unmeasured dofs. $s(t)$ (m/s^2) is a time-varying function of excitation (e.g., acceleration of shaker mass). In this context, $\boldsymbol{\varphi}(i)^T \mathbf{F}(t) = ms(t)\boldsymbol{\varphi}(i)^T \mathbf{a}$, where $\mathbf{a} = [a_1,...,a_n]^T$. The modal force and its FFT are given by

$$p_i(t) = r_i[\boldsymbol{\varphi}(i)^T \mathbf{a}]s(t) \tag{5}$$

$$P_{ik} = r_i[\boldsymbol{\varphi}(i)^T \mathbf{a}]S_k \tag{6}$$

where S_k is the FFT of $s(t)$ and

$$r_i = \frac{m}{\boldsymbol{\varphi}(i)^T \mathbf{M} \boldsymbol{\varphi}(i)} \qquad (7)$$

is the ratio of nominal mass to the modal mass. Substituting Equations (4) and (6) into Equation (3), we have

$$\mathcal{F}_k = \sum_{i=1}^{m} S_k h_{ik} r_i [\boldsymbol{\varphi}(i)^T \mathbf{a}] \boldsymbol{\varphi}(i) + \boldsymbol{\varepsilon}_k \qquad (8)$$

3. Mode shape scaling and parameterization scheme

Equation (8) is the basic equation that relates the data $\{\mathcal{F}_k\}$ and $\{S_k\}$ to modal parameters. The modal parameters include, for each mode, f_i (natural frequency), ζ_i (damping ratio), r_i (modal mass ratio) and $\boldsymbol{\varphi}(i)$ (mode shape); and parameters defining the statistical properties of the prediction error. The mode shape is subjected to a scaling constraint.

Using Equation (8) directly to identify the modal parameters does not lead to an effective scheme, primarily because of its quadratic dependence on mode shape $\boldsymbol{\varphi}(i)$, which is also subjected to scaling constraint. For example, Equation (8) will lead to a fourth-order dependence on mode shape in the objective function of a least square approach. Here, a mode shape scaling and parameterization scheme is proposed that allows the parameters to be determined efficiently in a globally identifiable manner and reduce the information required in the modal identification procedure. Beyond significance of computational nature, an interesting implication of the scheme is that the identification results are found to be invariant to the vector $\mathbf{a}$, which reflects the location and orientation of the artificial excitation. These practical implications shall be discussed in the Sections 4 – 6.

Conventionally, mode shapes may be scaled to be 1 at a particular dof or to have unit norm [13-16]. Neither of these can eliminate the quadratic dependence in Equation (8) on mode shape. Upon investigation of the mathematical structure of the problem, it is found that the following

scaling constraint allows the problem to be resolved while allowing for flexible implementation without prior information

$$\boldsymbol{\varphi}(i)^T \mathbf{a} = 1 \quad \text{for } i = 1,...,m \tag{9}$$

so that

$$\mathcal{F}_k = \sum_{i=1}^{m} S_k h_{ik} r_i \boldsymbol{\varphi}(i) + \boldsymbol{\varepsilon}_k \tag{10}$$

becomes a linear function of $\boldsymbol{\varphi}(i)$. Note that r_i and $\boldsymbol{\varphi}(i)$ are subjected to the constraint $\boldsymbol{\varphi}(i)^T \mathbf{a} = 1$. The formulation can be further simplified by combining them into an unconstrained vector

$$\boldsymbol{\varphi}_r(i) = r_i \boldsymbol{\varphi}(i) \tag{11}$$

so that

$$\mathcal{F}_k = \sum_{i=1}^{m} S_k h_{ik} \boldsymbol{\varphi}_r(i) + \boldsymbol{\varepsilon}_k \tag{12}$$

The parameters to be identified now comprise, for each mode i, f_i, ζ_i, $\boldsymbol{\varphi}_r(i)$ with no constraint; and parameters specifying the statistical properties of $\boldsymbol{\varepsilon}_k$. Once these parameters are identified, the modal mass ratio can be recovered by using Equation (9) and (11)

$$r_i = \boldsymbol{\varphi}_r(i)^T \mathbf{a} \tag{13}$$

4. Invariance to exciter configuration

In addition to providing an effective formulation for modal identification, the mode shape scaling and parameterization scheme in the Section 3 also leads to an interesting implication on how identification results depend on exciter configuration. Specifically, for given data ($\{\mathcal{F}_k\}$ and $\{S_k\}$), the information of $\mathbf{a}$, which is related to exciter location and orientation, is not needed to identify f_i, ζ_i and $\boldsymbol{\varphi}_r(i)$ as shown in Equation (12) and the same for other parameters related to the statistical modeling of prediction error. However, different values of $\mathbf{a}$ does affect the identification results because it affects the excitation magnitude. Although the scaling constraint on $\boldsymbol{\varphi}(i)$ in Equation (9)

depends on $\mathbf{a}$, $\boldsymbol{\varphi}(i)$ is in fact invariant because it has the same 'shape' as $\boldsymbol{\varphi}_r(i)$. To see this, $\boldsymbol{\varphi}(i) = r_i^{-1} \boldsymbol{\varphi}_r(i)$ makes the same hyper-angle with any vector $\mathbf{u}$ as $\boldsymbol{\varphi}_r(i)$:

$$\frac{\boldsymbol{\varphi}(i)^T \mathbf{u}}{\| \boldsymbol{\varphi}(i) \| \, \| \mathbf{u} \|} = \frac{r_i^{-1} \boldsymbol{\varphi}_r(i)^T \mathbf{u}}{r_i^{-1} \| \boldsymbol{\varphi}_r(i) \| \, \| \mathbf{u} \|} = \frac{\boldsymbol{\varphi}_r(i)^T \mathbf{u}}{\| \boldsymbol{\varphi}_r(i) \| \, \| \mathbf{u} \|} \tag{14}$$

The only parameter that is affected by $\mathbf{a}$ is the modal mass ratio $r_i = \boldsymbol{\varphi}_r(i)^T \mathbf{a}$.

5. Bayesian approach

To illustrate how the considerations in the previous sections enter into the formulation of a modal identification method, consider adopting a Bayesian approach for modal identification. Assume that the FFTs $\{\mathcal{F}_k\}$ on a selected frequency band with N_f frequencies (often around the modes of interest) are used for making inference and the prediction errors $\{\boldsymbol{\varepsilon}_k\}$ are independent and identically distributed with (unknown) power spectral density (PSD) S_e. Based on Equation (12), the set of modal parameters $\boldsymbol{\theta}$ should comprise $\{f_i, \zeta_i, \boldsymbol{\varphi}_r(i)\}_{i=1}^m$ and S_e, so that the likelihood function, i.e., the PDF of $\{\mathcal{F}_k\}$ for given $\boldsymbol{\theta}$ and $\{S_k\}$, can be determined. Assuming a constant prior PDF for $\boldsymbol{\theta}$, its posterior PDF is proportional to the likelihood function:

$$p(\boldsymbol{\theta} \,|\, \{\mathcal{F}_k\}, \{S_k\}) \propto p(\{\mathcal{F}_k\} \,|\, \boldsymbol{\theta}, \{S_k\}) = e^{-L(\boldsymbol{\theta})} \tag{15}$$

where

$$L(\boldsymbol{\theta}) = n N_f \ln \pi + n N_f \ln S_e + S_e^{-1} J(\boldsymbol{\theta}) \tag{16}$$

is the negative log-likelihood function (NLLF). $J(\boldsymbol{\theta})$ is given as

$$J(\boldsymbol{\theta}) = \sum_{i=1}^m \sum_k \left[\mathcal{F}_k - S_k h_{ik} \boldsymbol{\varphi}_r(i) \right]^* \left[\mathcal{F}_k - S_k h_{ik} \boldsymbol{\varphi}_r(i) \right] \tag{17}$$

It can be shown that [17] for sufficient data the posterior PDF of $\boldsymbol{\theta}$ can be approximated by a Gaussian PDF with mean equal to the most probable value (MPV) (minimum of the NLLF) and covariance matrix equal to the inverse of Hessian of the NLLF at the MPV. Clearly the MPV and covariance matrix do not depend on $\mathbf{a}$.

The MPV of S_e can be determined analytically in terms of the remaining parameters because the NLLF is of the form $a \ln S_e + b/S_e$ for some constant c, which has a minimum of $1 + \ln(b/a)$ at $S_e = b/a$. Substituting this into the NLLF gives a log of a quadratic function of $\varphi_r(i)$. Expanding the quadratic form of $J(\theta)$ in Equation (17), it becomes

$$J(\theta) = (\varphi_r :)^T \mathbf{A}(\{f_i, \zeta_i\})(\varphi_r :) - 2(\varphi_r :)^T \mathbf{B}(\{f_i, \zeta_i\}) + \sum_k \mathcal{F}_k^* \mathcal{F}_k \tag{18}$$

where

$$\mathbf{A}(\{f_i, \zeta_i\}) = \left[\sum_k |S_k|^2 \mathrm{Re}(\mathbf{h}_k^* \mathbf{h}_k) \right] \otimes \mathbf{I}_n \tag{19}$$

$$\mathbf{B}(\{f_i, \zeta_i\}) = \sum_k \mathrm{Re}(S_k^* \mathbf{h}_k^* \otimes \mathsf{F}_k) \tag{20}$$

'$\otimes$' denotes the Kronecker product and $\mathbf{I}_n \in R^{n \times m}$ is the identity matrix. $\mathbf{h}_k = [h_{1k}, ..., h_{mk}]$. $(\varphi_r :) \in R^{mn}$ denotes the 'vectorization', which is defined as

$$(\varphi_r :) = \begin{bmatrix} \varphi_r(1) \\ \vdots \\ \varphi_r(m) \end{bmatrix} \tag{20}$$

Minimizing the quadratic function in Equation (18) with respect to $(\varphi_r :)$ gives the MPV of $\varphi_r(i)$ in terms of the frequencies and damping. Consequently the MPV of θ can be determined efficiently by optimizing with respect to the frequencies and damping ratios only.

5.1. Posterior uncertainty of identified modal parameters

Using Bayesian approach, the uncertainty of the set of modal parameters can be obtained from the posterior covariance matrix $\mathbf{C}$, which is the inverse of the Hessian of the NLLF with respect to $\{\theta, S_e\}$. Since the cross derivatives of NLLF with respect to both θ and S_e are all zero, the Hessian of the NLLF with respect to $\{\theta, S_e\}$ is a block-diagonal $(2m + mn + 1)$-square matrix. The covariance matrix of θ and the variance of S_e can be evaluated separately as

$$\mathbf{C} = \begin{bmatrix} S_e \mathbf{H}_J^{-1} & \\ & \dfrac{\hat{S}_e^2}{nN_f} \end{bmatrix} \qquad (21)$$

where $\hat{S}_e$ is the MPV of S_e. $\mathbf{H}_J \in R^{(2m+mn)\times(2m+mn)}$ is the Hessian of $J(\boldsymbol{\theta})$. The posterior uncertainty of the identified natural frequencies and damping ratios can then be obtained from the covariance matrix $\mathbf{C}$.

5.2. Posterior uncertainty of mode shape

Suppose we want to obtain a mode shape scaled to have unit norm, i.e.,

$$\overline{\boldsymbol{\varphi}}(i) = \parallel \boldsymbol{\varphi}_r(i) \parallel^{-1} \boldsymbol{\varphi}_r(i) \qquad (22)$$

Substituting the MPV of $\boldsymbol{\varphi}_r(i)$ gives the MPV of $\overline{\boldsymbol{\varphi}}(i)$:

$$\hat{\overline{\boldsymbol{\varphi}}}(i) = \parallel \hat{\boldsymbol{\varphi}}_r(i) \parallel^{-1} \hat{\boldsymbol{\varphi}}_r(i) \qquad (23)$$

where a hat '^' denotes MPV. On the other hand, by means of perturbation, the posterior covariance matrix of $\overline{\boldsymbol{\varphi}}(i)$ can be obtained from that of $\boldsymbol{\varphi}_r(i)$ given by

$$\mathbf{C}_{\overline{\boldsymbol{\varphi}}(i)} = [\nabla\hat{\overline{\boldsymbol{\varphi}}}(i)] \, \mathbf{C}_{\boldsymbol{\varphi}_r(i)} \, [\nabla\hat{\overline{\boldsymbol{\varphi}}}(i)]^T \qquad (24)$$

where $\mathbf{C}_{\boldsymbol{\varphi}_r(i)}$ is the covariance matrix of $\boldsymbol{\varphi}_r(i)$, equal to the corresponding partition in the full covariance matrix of $\boldsymbol{\theta}$; and

$$\nabla\hat{\overline{\boldsymbol{\varphi}}}(i) = \parallel \hat{\boldsymbol{\varphi}}_r(i) \parallel^{-1} [\mathbf{I}_n - \hat{\overline{\boldsymbol{\varphi}}}(i)\hat{\overline{\boldsymbol{\varphi}}}(i)^T] \qquad (25)$$

is the gradient of $\overline{\boldsymbol{\varphi}}(i)$ with respect to $\boldsymbol{\varphi}_r(i)$ at MPV; $\mathbf{I}_n$ is $n \times n$ identity matrix. Clearly, the calculation of MPV and covariance matrix of $\overline{\boldsymbol{\varphi}}(i)$ does not require knowing $\mathbf{a}$.

5.3. Posterior uncertainty of modal mass

The modal mass ratio $r_i = \boldsymbol{\varphi}_r(i)^T \mathbf{a}$ is explicitly depends on $\mathbf{a}$. Its MPV and variance are given respectively by

$$\hat{r}_i = \hat{\boldsymbol{\varphi}}_r(i)^T \mathbf{a} \qquad (26)$$

$$\sigma_{r_i}^2 = \mathbf{a}^T \mathbf{C}_{\boldsymbol{\varphi}_{r(i)}} \mathbf{a} \qquad (27)$$

6. Insights and Practical Aspects

In this section we discuss the insight and practical aspects based on the formulation of modal identification with known forced vibration data in Sections 3, 4 and 5. Although the formulation in Section 5 is based on the Bayesian approach, the findings are general and applicable to the deterministic approach. The Bayesian approach allows quantification of the uncertainties associated with the identified modal parameters, by which the covariance matrix (Hessian of the NLLF at the MPV) provides a relationship between the provided information of the forced vibration test and the associated uncertainties of the identified modal parameters. This allows us to evaluate the accuracy of the identified modal parameters against the provided information.

Since the modal identification is achieved by minimizing the NLLF in Equation (16) through varying a set of unknown modal parameters $\boldsymbol{\theta}$, Equations (16) and (18) indicates the information required in the modal identification; and the covariance matrix reflects the impact of this information on the uncertainties of the identified modal parameters. When the mode shape is scaled to be 1 at a particular dof or to have unit norm, which is common in the literature [13-16], both of them lead to the quadratic dependence on mode shape as shown in Equation (8). In particular, the former explicitly assumes that the modal identification requires the information of exciter location and orientation for scaling the particular dof to be 1. However, the proposed mode shape scaling and parameterization scheme, i.e. Equation (9), explicitly shows that the required information in the identification of natural frequencies, damping ratio and mode shapes as Equation (8) can be reduced to Equation (12), in which the quadratic dependence in Equation (8) on mode shape is also eliminated. Since Equation (12) is invariant to the vector $\mathbf{a}$, the identification of natural frequencies, damping ratios and mode shapes only requires the measured sensor and exciter acceleration. The information of the exciter location and orientation is only required for recovering the modal mass ratios.

Within the context of Bayesian approach, since the covariance matrix, i.e. uncertainties, of the identified natural frequencies, damping ratios and mode shapes, is the Hessian of the NLLF at the MPV, this also implies that their uncertainties do not depend on the exciter configuration. This means that the accuracy of the exciter location and orientation does not affect the precision of the identified natural frequencies, damping ratios and mode shapes, and also the uncertainties of the results. However, as shown in Equation (27), the uncertainty of the modal mass ratio is still affected by the exciter configuration as vector **a** contains the information of the exciter configuration.

In practice, this means the natural frequencies, damping ratios and mode shapes can be identified without precisely placing the exciter in the required location and orientation in the forced vibration test unless the modal mass ratio is of primary interest. Table 1 summarizes the information required for identifying each modal parameter and quantifying the corresponding uncertainty in modal identification with known input.

It should be noted that although the modal identification procedure of the aforementioned modal parameters does not require knowing **a**, it will still affect the identification result. This is due to the fact that the excitation with different values of **a** will lead to different identification results as the excitation magnitudes are different. However, the differences are usually very small in practical engineering applications, for example, without placing the exciter precisely. This effect will also be investigated and discussed in the illustrative example in Section 7.

[Table 1: Summary of information required for identifying each modal parameter and quantifying the corresponding uncertainty in known input modal identification]

7. Illustrative example using synthetic data

To illustrate the aforementioned practical aspects and insights in Section 6, we consider a forced vibration test carried out on a two-dimensional two-story shear building. The height of the first and second stories is 4 m and 3 m, respectively. The inter-story stiffness of the first and second stories is 1.769×10^7 N/m and 1.244×10^7 N/m. The shear building has uniform mass 5600 kg at each floor.

The damping ratio is assumed to be 1% for all modes. The shear building has natural frequencies 3.261 Hz and 11.211 Hz. The simulation is performed at a sampling rate of 5000 Hz and the acceleration data is then decimated by 50 to a sampling rate of 100 Hz. An accelerometer is installed at each floor to measure the horizontal acceleration and the exciter is installed at the roof. The excitation signal is a pseudo-random excitation with flat root PSD from 0.1 Hz to 15 Hz. The measured data covers 10 s before the shaker is turned on, 140 s forced vibration during which the shaker is turned on, and 35 s free vibration after the shaker is turned off, that is, a total of 185 s. The measured acceleration is contaminated by i.i.d. Gaussian white noise with a root PSD of 1×10^{-7} $g / \sqrt{Hz}$. Figure 1 shows the root PSD spectra of the measured acceleration responses from the two-story shear building. Obviously both modes are adequately excited as indicated by their resonance peaks apparent.

[Figure 1: Root power spectral density spectra (solid line: first floor data; dashed line: second floor data)]

7.1. Identification results using proposed mode shape scaling and parameterization scheme

The modal identification is then carried out using the fast Bayesian FFT modal identification method with proposed mode shape scaling and parameterization scheme in Equation (9). The bars in Figure 1 indicate the frequency band within that the FFT data used for the modal identification. In this study, the two vibration modes are identified separately with a single mode ($m = 1$) assumed within each band.

To carry out the modal identification using the proposed mode shape scaling and parameterization scheme, it requires the FFT data of sensor and exciter accelerations within the selected frequency band. The f_i and ζ_i can be identified by numerically minimizing J in Equation (18). After that the $\varphi_r(i)$ can be identified using Equation (18) again with f_i and ζ_i being their MPV values. In identifying these modal parameters, the information of vector $\mathbf{a}$ is not required. The

vector **a** is only required if the modal mass ratio is also of the interest and it can be recovered from the MPV of $\varphi_r(i)$ using Equation (26).

The posterior uncertainty of the identified modal parameters can be obtained using Bayesian approach. Once the MPV of the modal parameters are obtained, the posterior uncertainties can be calculated from the covariance matrix with respect to the set of modal parameters $\boldsymbol{\theta}$ using Equation (21). The uncertainties of the natural frequencies, damping ratios and mode shapes can be determined without knowing the vector **a** as shown in Sections 5.1 and 5.2. The same as calculating the MPV, the vector **a** is only required to determine the uncertainty of modal mass ratio using Equation (27).

The identified natural frequencies, damping ratio, modal mass ratio and the corresponding posterior coefficient of variation (c.o.v.) are summarized in Table 2. The posterior c.o.v. is the square root of the posterior variance divided by the MPV. The results show that the identified modal parameters agree very well with their exact values. The posterior c.o.v.s of the natural frequencies are smaller than that of damping ratios and modal mass ratios. Figure 2 shows the identified mode shapes. There is good agreement between the identified mode shape and their exact counterparts.

[Table 2: Summary of modal identification results without exciter angle error]

[Figure 2: Identified mode shape (solid line: most probable value; dashed line: exact value)]

7.2. *Effect of exciter angle error*

In practical situation there is always error in the measurement and excitation direction. For example, the exciter may not be installed perfectly at the expected angle, i.e. not completely align with the expected dof. In this situation, the actual magnitude of the excitation applied at the expected dof is smaller than the expected magnitude by a factor of $\cos(\phi_e)$, where ϕ_e is the angle error of the

exciter direction. $\phi_e = 0°$ means no error in the exciter direction. In this study, different angle errors in the exciter direction, $\phi_e = 10°$, 20°, 30° and 40° are considered. In the simulations of these cases, the force of the exciter is factorized by $\cos(\phi_e)$, however, the modal identifications are still carried out using **a** = [0;1]. This simulates the angle error of the exciter direction in the modal identification and demonstrates the independence of vector **a** in identifying natural frequencies, damping ratios and mode shapes.

The identified modal parameters are summarized in Table 3. The percentage differences between the identified modal parameters obtained from data with and without exciter angle error are also shown in the Table 3. The results show that when the exciter angle error increases, the identified natural frequencies and damping ratios still agree very well with the values identified using data without the exciter angle error. The maximum percentages difference for natural frequencies and damping ratios is 0% and -0.052%, respectively. For the identified modal mass ratios, the results in Table 3 show that the percentage differences between the identified modal mass ratios from the data with and without exciter angle error are significantly affected by the magnitude of the exciter angle error. The maximum percentage difference for the modal mass ratio is 23.393%. This indicates that exciter angle error only affects the identification of modal mass ratio. This is consistent with the findings obtained and discussed in Section 6.

[Table 3: Modal identification results and percentage difference between identified results using data with and without exciter angle error]

The associated uncertainties of the identified modal parameters are quantified as posterior c.o.v. values and summarized in Table 4. In general, the posterior c.o.v. slightly increases with the exciter angle error. The signal-to-noise ratio of the measured accelerations is reduced due to the exciter angle error. With the exciter angle error, the excitation does not completely align with the expected dof, and hence, the magnitude applied at the expected is reduced. This means that

although the accuracy of determining the MPVs and uncertainties of the natural frequencies, damping ratios and mode shapes does not depend on the accuracy of the exciter location and orientation, it still depends on how well the subject vibration mode is excited, as it affects the signal-to-noise ratio of the measured acceleration. Therefore the exciter still needs to be installed correctly at the required position, but it does not require very accuracy for identifying the natural frequencies, damping ratios and mode shapes. This significantly simplifies the field testing procedure as it is always difficult to accurately install the exciter at the required position in the field testing condition. However, if the primary objective of the forced vibration test is to determine the modal mass, the exciter still needs to be placed accurately at the required position.

[Table 4: Posterior c.o.v. of the modal identification results using data with and without exciter angle error]

8. Conclusions

This paper has proposed a mode shape scaling and parameterization scheme for identifying modal parameters. Besides significance of computational nature, the formulation has provided insights into the relationship between the identified modal parameters and information required in a forced vibration test. An illustrative example using synthetic data has been provided in this study. It is found that only the sensor and exciter acceleration are required for identifying the natural frequencies, damping ratios and mode shapes. An appropriate mode shape scaling scheme could reduce the information required in the modal identification, and hence, the procedure of the forced vibration can be significantly simplified. However, to determine the modal mass ratio, accurate placement of the exciter is still essential. It is hoped that these findings can improve understanding of some practical aspects in carrying out forced vibration tests with known input, such as those with electrodynamic shaker or impulse hammer.

9. Acknowledgement

10. References

1. Yang, J.H., Lam, H.F., Hu, J. (2015). Ambient vibration test, modal identification and structural model updating following Bayesian framework. International Journal of Structural Stability and Dynamics, 15(7):1540024.

2. Devin, A., Fanning, P.J., Pavic, A. (2015). Modelling effect of non-structural partitions on floor modal properties. Engineering Structures, 91:58-69.

3. Ng, C.T. (2014). Application of Bayesian-designed artificial neural networks in Phase II structural health monitoring benchmark studies. Australian Journal of Structural Engineering, 15(1):27-36.

4. Ashebo, D.B., Chan, T.H.T., Yu, L. (2007). Evaluation of dynamic loads on a skew box girder continuous bridge Part I: field test and modal analysis. Engineering Structures, 29(6):1052-1063.

5. Chen, W.H., Lu, Z.R., Lin, W., Chen, S.H., Ni, Y.Q., Xia, Y., Liao, W.Y. (2011). Theoretical and experimental modal analysis of the Guangzhou New TV Tower. Engineering Structures, 33:3628-3646.

6. Lam, H.F., Hu, J., Yang, J.H. (2017). Bayesian operational modal analysis and Markov chain Monte Carlo-based model updating of a factory building. Engineering Structures, 132: 314-336.

7. Memari, A.M., Aghakouchak, A.A., Ghafory Ashtiany, M. and Tiv, M. (1999). Full-scale dynamic testing of a steel frame building during construction. Engineering Structure, 21: 1115-1127.

8. Halling, M.W., Muhammad, I. and Womack, K.C. (2001). Dynamic field testing for condition assessment of bridge bents. Journal of Structural Engineering, ASCE, 127(2): 161-167.

9. Burgueno, R., Karbhari, V.M., Seible, F. and Kolozs, R.T. (2001). Experimental dynamic characterization of an FRP composite bridge superstructure assembly. Composite Structures, 54: 427-444.

10. Bai, Y. and Keller, T. (2008). Modal parameter identification for a GFRP pedestrian bridge. Composite Structures, 82: 90-100.

11. Trifunac, M.D. (1972). Comparison between ambient and forced vibration experiments. Earthquake Engineering and Structural Dynamics, 1: 133-150.

12. Yu, E., Whang, D.H., Conte, J.P., Stewart, J.P. and Wallace, J.W. (2005). Forced vibration testing of buildings using the linear shaker seismic simulation (LSSS) testing method. Earthquake Engineering and Structural Dynamics, 34: 737-761.

13. Vanik, M.W., Beck, J.L. and Au, S.K. (2000). Bayesian probabilistic approach to structural health monitoring. Journal of Engineering Mechanics, ASCE, 126(7): 738-745.

14. Yuen, K.V. and Katafygiotis, L.S. (2002). Bayesian modal updating using complete input and incomplete response noisy measurement. Journal of Engineering Mechanics, ASCE, 128(3): 340-350.

15. Au, S.K. and Ni, Y.C. (2013). Fast Bayesian modal identification of structures using known single-input forced vibration data. Structural Control and Health Monitoring, 21(3): 381-402.

16. Reynders, E., Maes, K., Lombaert, G. and De Roeck, G. (2016). Uncertainty quantification in operational modal analysis with stochastic subspace identification: Validation and applications. Mechanical Systems and Signal Processing, 66-67: 13-30.

17. Katafygiotis, L. and Beck, J. (1998). Updating models and their uncertainties II: Model identifiability. Journal of Engineering Mechanics, ASCE, 124(4): 463-467.
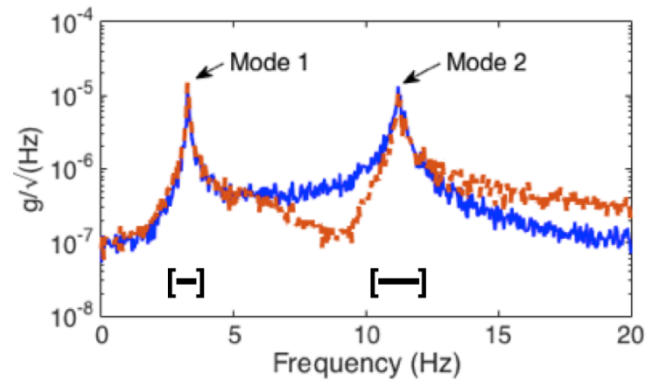
Figure 1: Root power spectral density (solid line: first floor data; dashed line: second floor data)
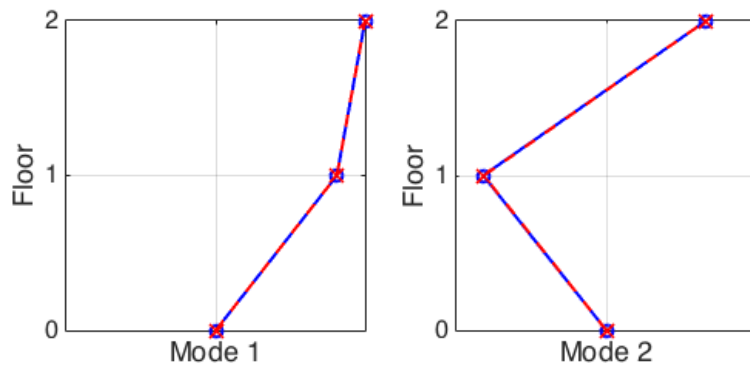

Figure 2: Identified mode shape (solid line: most probable value; dashed line: exact value)

Table 1: Summary of information required for identifying each modal parameter and quantifying the corresponding uncertainty in known input modal identification

Modal parameter	Required information in forced vibration test
Natural frequency	Sensor and exciter acceleration only
Damping ratio	Sensor and exciter acceleration only
Mode shape	Sensor and exciter acceleration only
Modal mass ratio	Sensor and exciter acceleration & Precise exciter location and orientation

Table 2: Summary of modal identification results without exciter angle error

		Mode 1	Mode 2
f	Exact (Hz)	3.261	11.211
	MPV (Hz)	3.261	11.211
	c.o.v. (%)	0.0017	0.0096
ζ	Exact (%)	1.000	1.000
	MPV (%)	1.002	1.002
	c.o.v. (%)	0.233	0.144
r	Exact (10^{-4})	14.434	9.495
	MPV (10^{-4})	14.442	9.497
	c.o.v. (%)	0.179	0.136

Table 3: Modal identification results and percentage difference between identified results using data with and without exciter angle error

Exciter angle error	Mode	f(Hz)	Diff. of f (%)	ζ (%)	Diff. of ζ (%)	r (10⁻⁴)	Diff. of r (%)
10°	1	3.261	0	1.002	-0.00	14.203	1.520
	2	11.211	0	1.002	-0.00	9.353	1.519
20°	1	3.261	0	1.002	-0.01	13.552	6.034
	2	11.211	0	1.002	-0.01	8.924	6.030
30°	1	3.261	0	1.002	-0.03	12.489	13.405
	2	11.211	0	1.002	-0.03	8.225	13.396
40°	1	3.261	0	1.002	-0.05	11.046	23.409
	2	11.211	0	1.002	-0.05	7.275	23.393

Note: Diff. (%) is the percentage difference of the identified values between the results of with and without exciter angle error

Table 4: Posterior c.o.v. of the modal identification results using data with and without exciter angle error

Exciter angle error	Mode	c.o.v. of f (%)	c.o.v. of ζ (%)	c.o.v. of r (%)
10°	1	0.0017	0.233	0.182
	2	0.0010	0.144	0.138
20°	1	0.0018	0.244	0.190
	2	0.0010	0.151	0.145
30°	1	0.0020	0.265	0.207
	2	0.0011	0.164	0.157
40°	1	0.0022	0.300	0.234
	2	0.0013	0.185	0.178